Universidad de Navarra

Development of G9a-targeted BioPROTACs based on peptides and nanobodies

Faculty of Sciences

Therapeutic Innovation Program (CIMA)

Final Degree Project

Biochemistry + Science and Business Program

2022-2023

Author: Lucía Gómez Vegas

Tutors: Dr. Antonio Pineda Lucena, Vianca Ibarra García

INDEX

ABSTRACT

This project arose motivated by the high incidence that neoplastic pathologies have nowadays, and therefore by the need that our society has to find a solution against them. The main objective of this research was to identify specific peptides and nanobodies against G9a methyltransferase, whose role in cancer is to introduce epigenetic modifications to silence tumor suppressor genes. The strategy followed focuses on degrading this enzyme through the Biological Proteolysis Targeting Chimera (BioPROTAC) system, made up of either the aforementioned peptides or nanobodies. A search for these specific molecules was carried out using phage display, to find the most specific candidates against the previously produced and purified G9a. Later, the binding affinity of the selected clones was evaluated, the BioPROTAC construct was designed, and immunocytochemistry (ICQ) was performed to check their cellular internalization. In short, it was possible to select 3 peptide clones and 16 nanobodies with a good affinity for G9a, in addition to designing a system capable of being introduced into the tumor cell. This represents a project of Targeted Protein Degradation (TPD) for drug discovery with its main objectives met. Furthermore, this study will facilitate future investigations aimed at confirming the efficacy of the system to degrade the enzyme, in order to conduct additional testing of its therapeutic effect.

Keywords: G9a, methyltransferase, BioPROTAC, phage display, Targeted Protein Degradation, drug discovery.

1. INTRODUCTION

This Final Degree Project is framed in the context of cancer pathogenesis and the multistep process of human tumor development. It is well known that cancer is positioned as a leading cause of death worldwide (1). The main concern, however, remains in its increasing incidence among high-income countries where lifestyle behaviors such as tobacco use, or physical inactivity are common (2). Therefore, it is no wonder that the recent trend of governments and institutions is to invest in and provide more funding for cancer research (3). In short, it is an area of study with great interest and precisely the main motivation of this work.

Neoplastic diseases comprise a wide variety of molecular mechanisms, and the exact etiology of carcinogenesis is complex. However, it is known that cancer has its origin in both genetic and epigenetic modifications that alter the expression of several genes and growth factors (4). In this case, attention is paid to epigenetic events that increase the probability of human tumor development (5,6).

The epigenetic modifications in DNA and histones play an important role in the regulation of processes such as replication, transcription, or DNA repair (6). In DNA, cytosine residues in CpG dinucleotides can be methylated, whereas the N-terminal tails of histone proteins can also undergo a variety of changes such as acetylation, methylation, or phosphorylation (7). These modifications therefore can have a direct impact on chromatin structure and gene expression, consequently, it is not surprising that epigenetics has a narrow relationship with aberrant gene expression patterns observed in cancer.

According to several studies, some cancer cells express unusually high levels of methyltransferases, whose activity of methylation sometimes acts over tumor suppressor genes for their silencing (8,9). Functional loss of these genes via methylation of their CpG-island promoter means that negative control of cell proliferation is no longer available and malignant transformation becomes more likely to occur (10,11).

There are several proteins involved in processes of epigenetic modifications over either DNA or histones. As stated before, the N-terminal tails of histones (proteins that give structural support and protection to DNA) are susceptible to epigenetic modifications. On the one hand, acetylation of histones is related to weaker interaction with DNA, which allows active transcription (12). Acetyl groups are incorporated into lysine groups (K) of histones 3 and 4

(H3 and H4, respectively). On the other hand, methylation of H3 and H4 can produce either transcription activation or repression, depending on the site of methylation (13).

Some of the histone modifications have been proven to be more usual in the cancer cell epigenome. For instance, deacetylation of histones H3 and H4, loss of H3K4 trimethylation, and gain of H3K9 methylation are common patterns in cancer cells (11). EHMT2 (Euchromatic histone-lysine N-methyltransferase 2), also known as G9a, is responsible for catalyzing the H3K9 mono- and dimethylation and is involved in tissue differentiation, embryonic development, cancer cell proliferation and cancer cell invasion (14).

It has been found that different solid tumor types over-express the protein G9a, including lung, ovarian, esophageal, hepatocellular, brain cancers, and multiple myeloma. In addition, it also has been established as a poor prognosis marker (15–17). Over-expression of G9a is associated with higher methylation in tumor suppressor genes, leading to their transcriptional silencing according to several Genome Wide Analysis Studies (18). This results in more aggressive cancer phenotypes that have greater invasion and metastasis capability (19,20).

Several studies have already shown that G9a inhibition can delay tumor development by decreasing cancer cell proliferation (21) and blocking tumor metastasis (22,23). Some examples of G9a inhibitors include UNC0638, BIX-01294, A-366 and CM-272. These compounds have been shown to exhibit potent inhibitory effects of G9a in vitro and in vivo (24–27), and have demonstrated promising results in preclinical studies.

However, several proteins have limited binding sites considered as “undruggable” target to small molecules. Proteolysis-targeting chimera (PROTAC) represents a significant category of molecules that could facilitate the modulation of such proteins via Targeted protein Degradation (TPD) (28).

PROTAC molecules are bifunctional systems composed of a ligand of the protein of interest (POI) and a ligand of an E3 ubiquitin ligase (such as Von Hippel-Lindau tumor suppressor ((VHL) or Cereblon (CRBN)); both ligands are connected by a linker sequence. After binding to the POI, the PROTAC is able to recruit E3 for POI ubiquitination (29). This allows targeting and directing certain proteins toward the endogenous proteasome degradation system (**Figure**

1). The ubiquitination process begins with a ubiquitin tag that binds to an E1 enzyme, which is then transferred to an E2 enzyme and later delivered to the POI by an E3 enzyme. The ubiquitinated protein is finally specifically recognized by proteasome and degraded into peptides by various enzymes (30).

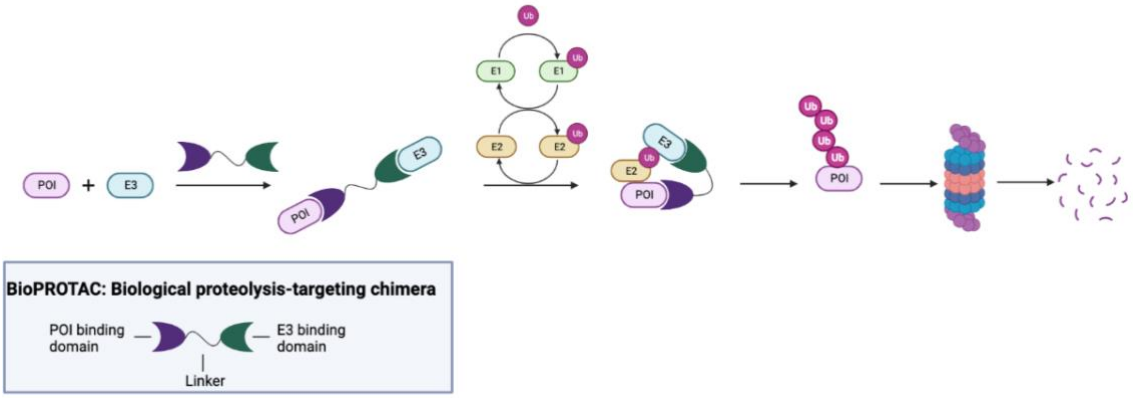

Figure 1. Schematic representation of how a PROTAC system works*. It is composed of a POI binding domain linked to an E3 binding domain by a linker. Once the POI and E3 are bound to the system, ubiquitination of the protein begins. Firstly, an E1 enzyme recruits a ubiquitin tag and then transfers it to an E2 enzyme. The latter enzyme then delivers the tag to the E3 enzyme, and the whole process is repeated in various cycles. In the end, the POI ends up with a polyubiquitin tail bound to it, which is specifically recognized by the proteasome and degraded into peptides by various enzymes*.

Currently, TPD technologies have moved from academia to industry, with various companies including preclinical and early clinical programs in their pipeline (**Table 1**). Novel PROTAC-based therapies are already being used; they combine the aforementioned E3 ubiquitin ligase with different molecule types that bind the POI.

Company	Degrader	Target	Indications	E3 ligase	ROA	Highest clinical phase
Arvinas	ARV-110	AR	Prostate cancer	CRBN	Oral	Phase II
Arvinas/Pfizer	ARV-471	ER	Breast cancer	CRBN	Oral	Phase II
Accutar Biotech	AC682	ER	Breast cancer	Undisclosed	Oral	Phase I
Arvinas	ARV-766	AR	Prostate cancer	CRBN	Oral	Phase I
Bristol Myers Squibb	CC-94676	AR	Prostate cancer	VHL	Intravenous	Phase I
Dialectic Therapeutics	DT2216	BCL	Liquid and solid tumors	Undisclosed	Intravenous	Phase I
Foghorn Therapeutics	FHD-609	BRD9	Synovial sarcoma	Undisclosed	Oral	Phase I
Kymera/Sanofi	KT-474	IRAK4	Autoimmune diseases (AD, HS, RA)	CRBN	Intravenous	Phase I
Kymera	KT-413	IRAK4	Diffuse large B cell lymphoma	Undisclosed	Undisclosed	Phase I
Kymera	KT-333	STAT3	Liquid and solid tumors	CRBN	Oral	Phase I
Nurix Therapeutics	NX-2127	BTK	B cell malignancies	CRBN	Oral	Phase I
Nurix Therapeutics	NX-5948	BTK	B cell malignancies and autoimmune diseases	CRBN	Oral	Phase I
C4 Therapeutics	CFT8634	BRD9	Synovial sarcoma	CRBN	Oral	IND-e
C4 Therapeutics	CFT8919	EGFR	Non-small-cell lung cancer	CRBN	Oral	IND-e
Cullgen	CG001419	TRK	Cancer and other indications	CRBN	Oral	IND-e

Table 1. Heterobifunctional PROTAC targeted protein degraders in clinical development. *Companies with protein targeted PROTACs in clinical development (Table adapted from* (31)*).*

The PROTAC system offers numerous potential advantages; this technology can act over the POI, even if the PROTAC is in sub-stoichiometric concentrations because it is recycled after one round of protein degradation (29) (**Figure 2**). This constitutes a great advantage of protein degraders over protein inhibitors because the recycling process allows a PROTAC's degradation concentration 50 (DC_{50}) to be significantly lower than an inhibitor's inhibitory concentration 50 (IC_{50}) value. Following the same idea, the POI and PROTAC only require a transient binding, so this provides an opportunity to overcome mutation-directed drug resistance (32).

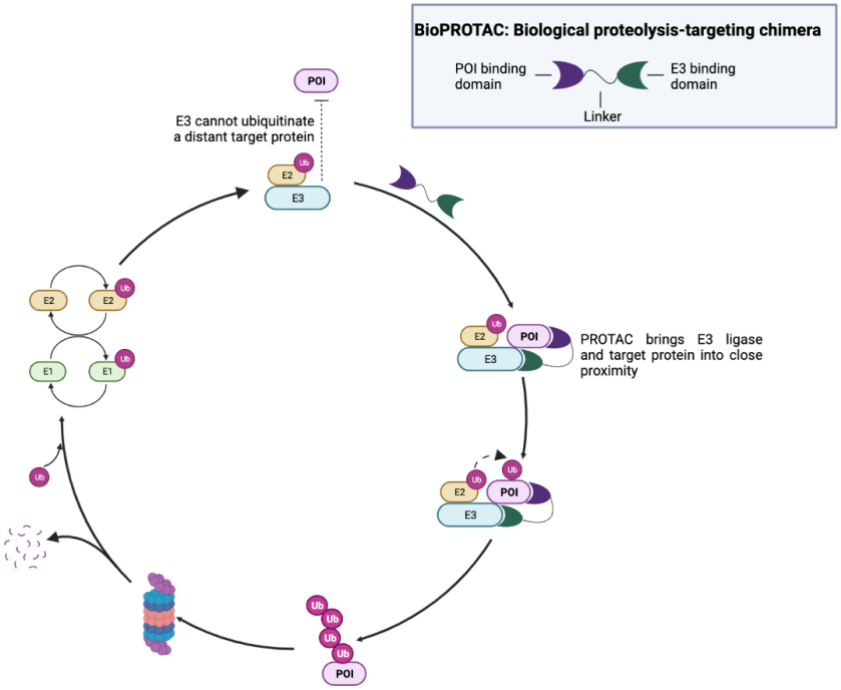

Figure 2. Life-cycle of a BioPROTAC molecule. *After one round of protein degradation, the BioPROTAC molecule is recycled in order to transfer various ubiquitin tags to the POI. The proteasome recognizes the protein when it is polyubiquitinated.*

However, developing a traditional high-affinity small molecular ligand for PROTACs can be a time-consuming and laborious process and may not be feasible for many potential targets due to the lack of small molecule binding sites. To address these issues, variants of PROTAC systems have been developed, such as LYTACs (lysosome-targeting chimeras) (33), AbTACs (antibody-targeting chimeras) (34), and O'PROTACs (oligonucleotide-based PROTACs) (35).

Another of those variants is called BioPROTAC (Biological Proteolysis Targeting Chimera) (**Figure 2**), which is a type of chimeric fusion protein that consists of a target binder, typically a peptide or a miniprotein, and an E3 ligase function domain. BioPROTACs recruit target proteins to the fused E3 ligase through the target binder, enabling selective degradation of the target protein.

In short, implementation of BioPROTAC technology would allow specific targeting and degradation of G9a, promoting the re-expression of tumor suppressor genes that had been silenced by epigenetic modifications. Due to the pathological context of cancer in which G9a is overexpressed, a traditional protein inhibitor may not achieve a therapeutic effect because of the high abundance of the protein and the inability to reduce its quantity. Hence the importance of using PROTACs in this context, as this system does not inhibit but rather degrades the protein, causing its quantity to decrease. Furthermore, it is a circular ubiquitin-proteasome system (UPS) that is recycled and can continue to act in several cycles of protein degradation. This results in new potential therapeutic approaches for cancer, based on Targeted Protein Degradation (TPD) technology.

2. OBJECTIVES

Primary objectives

The main goal of this study is to identify small peptides and nanobodies against G9a and design protein degradation complexes (BioPROTACs) that would efficiently penetrate in tumor environments.

Secondary objectives

- Produce and purify the protein G9a, followed by activity assays to measure G9a activity.
- Identify peptides and nanobodies against G9a using Phage Display Libraries.
- Characterize small peptides and nanobodies against G9a.
- Evaluate the effect of small peptide BioPROTAC construct, testing it in different tumor cell lines.

3. MATERIALS AND METHODS

The project started with G9a production in bacteria and its subsequent purification and activity measurement. Once the target protein had been produced, panning rounds were performed in order to select G9a-specific peptides and nanobodies. That specificity was proven by phage ELISA and screening assays; the selected peptide and nanobody clones were sequenced and synthesized for BioPROTAC construction. Later on, immunocytochemistry was performed to check cell internalization. The schematic workflow of the project is specified in **Figure 3**.

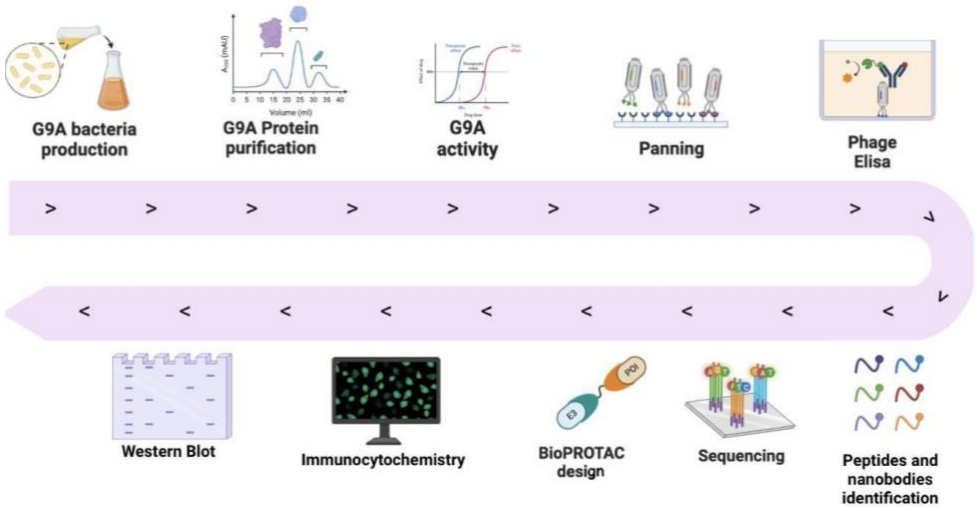

Figure 3. Schematic summary of the workflow followed in the project. *G9a was obtained through bacteria production and chromatographic purification. The active enzyme was then used for selection of specific peptides and nanobodies against it.*

3.1 Production of G9a

The first step carried out in the project was the recombinant expression of the target protein (G9a) in *Escherichia coli* (*E. coli*), due to its easy handling and fast expression process. An *in silico* DNA fragment encoding human G9a with polyhistidine tail at the N-terminus was designed, and later synthesized into the pET-15b vector of expression by GenScript® (**Figure 4**). Later, production of the protein was achieved using *E. coli* BL21 strain. Transformation of the bacteria with G9a plasmid was carried out by two different procedures: heat shock and electroporation (following standardized procedures found in bibliographical research).

In the case of electroporated bacteria, it is necessary to induce the competent state in order to introduce foreign DNA with high efficiency into them. To achieve this, bacterial cultures of *E. Coli* BL21 strain (Merck KGaA®) were treated while being in logarithmic growth phase, with chemical agents (10% glycerol) that are able to weaken the structure of the bacterial cell wall. Therefore, DNA derived from different sources can be introduced into cells. The electrocompetent bacteria BL21 were stored in aliquots at -80ºC with 30% glycerol.

a.

HHHHHHSSGTEKIICRDVARGYENVPIPCVNGV
DGEPCPEDYKYISENCETSTMNIDRNITHLQHC
TCVDDCSSSNCLCGQLSIRCWYDKDGRLLQEFN
KIEPPLIFECNQACSCWRNCKNRVVQSGIKVRL
QLYRTAKMGWGVRALQTIPQGTFICEYVGELIS
DAEADVREDDSYLFDLDNKDGEVYCIDARYYGN
ISRFINHLCDPNIIPVRVFMLHQDLRFPRIAFF
SSRDIRTGEELGFDYGDRFWDIKSKYFTCQCGS
EKCKHSAEAIALEQSRLARLDPHPELLPELGSL
PPVNT*

b.

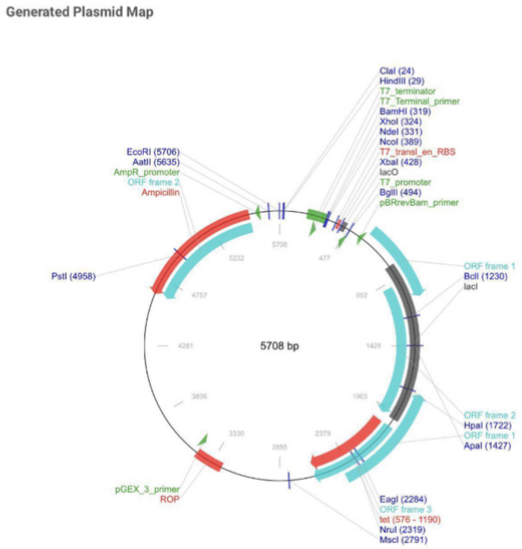

Figure 4. Sequence of the G9a cloned in the vector pET-15b*. The vector provided by GenScript® was designed to express catalytic domain of G9a and polyhistidine tag with ampicillin resistance in order to select transformed colonies. a: synthesized G9a sequence. b: pET-15b vector of expression, IPTG inducible.*

Once the competent bacteria were achieved, transformation with G9a plasmid was performed by electroporation and heat shock. Transformed bacteria were grown in 1L LB medium (Teknovas, Condalab) with 100 µg/mL of ampicillin, at 37ºC until OD_{600} (optic density) 0.6 was achieved. Later, different concentrations of isopropyl-β-D-1-thyogalactopyranoside (IPTG #12481C50, Gold Biotechnology) were tested for protein expression optimization. Once the protein was produced, lysis of the bacteria was performed by high pressure in French Press and 2 µL lysozyme. After lysis, the supernatant where G9a remained, was centrifuged, and filtered to initiate the purification process.

3.2 Purification of G9a

In a first step, an Immobilized Metal Affinity Chromatography (IMAC) was performed using the HiTrap Chelating column with nickel (Ni^{2+}). G9a was purified based on the affinity that polyhistidine-tagged proteins have for metal ions like Ni^{2+} (36). Elution of the protein from the column was performed with a competitive inhibitor for histidine-tagged proteins: imidazole 750mM was used (Imidazole C3H4N2 Sigma-Aldrich®, # 56750). A linear gradient of the inhibitor (0%-4%-20%-40%-100%) was used in order to achieve properly separated peaks in the chromatogram. Subsequently, the purified IMAC protein was repurified by size exclusion using Superdex-200 to ensure the required purity.

Four different G9a batches were produced and the protein of each of them was later quantified by a BCA assay. In the first place, a standard curve was prepared using serial dilutions of BCA protein [1µg/µL] in Milli-Q® water. Then, a sample of each of the batches was also diluted in water. Finally, 100µL of the working reagent from BCA assay kit (Thermofischer®) were added in each well, and absorbance was measured at 590 nm allowing the interpolation of sample values in the standard curve.

3.3 G9a activity assay

After that, the activity of the purified protein was subsequently verified by a biochemical assay, which measures the enzymatic activity based on time-resolved fluorescence energy transfer (TR-FRET). The enzyme activity assay was carried out with the same amount of G9a (0.1 nM) per well, and decreasing concentrations of the selective inhibitor CM-272 in order to obtain an IC50 value that correlates with the activity. The reaction took place at room temperature (RT) for 1h, and enzyme activity was stopped by adding 5 µL of cryptate-labeled anti-dimethyl-histoneH3K9 antibody. Then, 5 µL of streptavidin XL665 beads were added and the plate was left incubating at RT for 1h. After that, fluorescence was measured at 620 nm and active fractions of G9a were collected and quantified by the BCA method. The final aliquots of G9a were stored at -80ºC for future applications. Finally, the antigen was lyophilized and sent to Montevideo, Uruguay, at a controlled temperature for further inoculation into llamas to generate nanobodies and subsequent use for panning (phage display) assays.

3.4 Peptide identification

Phage display is a molecular biology technique used to study protein-protein, protein-DNA, or protein-peptide interactions. It involves the use of filamentous bacteriophages such as M13 helper phage to display peptides or proteins on their surface, allowing for the selection and identification of specific protein or peptide sequences that bind to a target molecule of interest (G9a, in this case).

The Ph.D.-7 peptide library (NEB, New England Biolabs, USA, E8100S) was acquired and used to evaluate anti-G9a peptides following the manufacturer's recommendations. Briefly, 10 µg of active G9a (previously tested) were used for coating the plate at a final concentration of 100 µg/mL overnight, at 4ºC in a wet container. The phage display process was carried out by first blocking with 300 µL PBS-BSA for 1h at RT, and then incubating with the phage library presenting the random peptide library $2x10^{11}$ (1h, at RT). The unbound phages were discarded, and the bound phages were vigorously washed with PBS saline solution (PBS+0.1% Tween 20) to avoid nonspecific binding to the target. On the other hand, the phages that remained bound after the washings were eluted by evaluating different strategies of HCL, Trypsin, and G9a inhibitor CM-272. Finally, the phages were tittered using LB/IPTG/X-gal plates with serially diluted phages. A second and third round of panning was performed using more stringent conditions, following the standard recommendations described, where the amount of protein was decreased, and the washes were increased.

Between each round of panning, the titer of the phages used (input, **Figure 5, step 1**) and the bound and eluted phages (output, **Figure 5, step 3**) were calculated. Every panning round starts with an input of 2×10^{11} phages containing about 2×10^{9} clones or peptides; the commercial library already contained 2×10^{11} phages. In addition, the eluted phages of each round were amplified by ER2738 bacterial strain culture (37ºC for 4.5 h) and precipitated using ⅙ volume of 20% PEG/2.5 M NaCl (Promega® # V3011) for 2h at 4ºC. After 3 rounds of analysis as recommended, a Phage ELISA was carried out to select and choose the peptide sequences to be sequenced and used in subsequent assays.

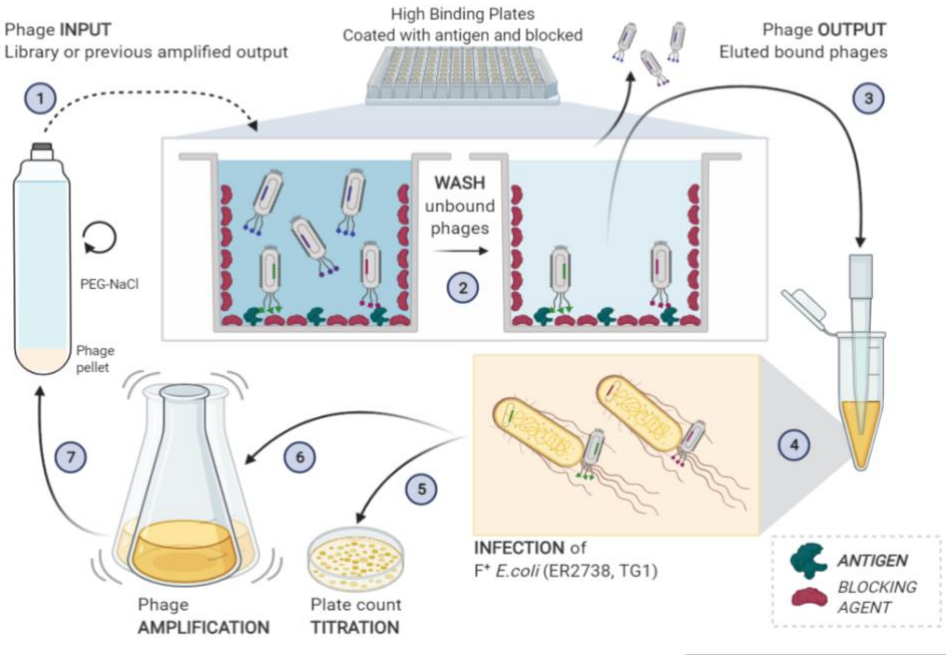

Figure 5. Process of a phage display round step by step. *Firstly, the phage input is put onto the target protein-coated plate (1). Unbound phages are washed (2) and the bound phages or output are collected (3). The phage output is subsequently amplified and titrated by E. Coli infection (4, 5 and 6), obtaining the phage input of the next panning round.*

It is worth noting that before the third panning round, a prepanning was performed in order to increase the specificity of the peptides selected. The prepanning round was carried out equally to other rounds, with the difference that the plate was not coated with G9a. The coating was done with a different protein that had also been purified by its histidine tag, to avoid selecting peptides that recognize the tag and not the catalytic domain of the protein.

3.5 Phage ELISA and peptide characterization

As previously stated, the affinity of peptides obtained from the first Ph.D.-7 library (NEB, New England Biolabs, USA, E8100S) was evaluated by phage ELISA, using G9a as the coating antigen and 1% BSA as the blocking solution. Once the clones were enriched, the peptides were individually characterized to determine those with the best affinity. Each clone was inoculated in 20 mL of ER2738 bacteria culture, and left incubating at 37°C until OD_{600} 0.6 was reached. At the same time, the plate was coated with 100 µL G9a at 0.1 M overnight. The phages of each clone were then precipitated with 20% PEG and put individually over the plate. Later, an anti-M13-peroxidase antibody (Sinobiological®) was added at 1:10000 dilution, as well as a

tetramethylbenzidine (TMB) substrate reagent (BD OptEIA™) for plate reveal. The peptides that were specific for the antigen of interest were considered 'positive' and the non-specific peptides were considered 'negative'. This classification was made according to the reveal color they showed (positive clones) or did not show (negative clones), and to their absorbance value at 450 nm.

The phages that showed the highest binding against G9a were sequenced for subsequent synthesis of the selected peptides. Once synthesized, the peptides were individually evaluated using microscale thermophoresis (MST) as a biophysical characterization tool on NanoTemper®. MST was used to determine the affinity of the peptides for the target protein, obtaining the dissociation constant (Kd) of each one. For this, the peptides were labeled with His-Tag Labeling Kit RED-tris-NTA 2nd Generation. In this assay, G9a was used at a final concentration of 25nM, while the final concentration of the peptides was 20mM. All measurements were performed in duplicate, with 100% excitation power, and 60% MST power.

3.6 Nanobodies generation and clone screening

On the other hand, G9a inoculation in llamas was carried out in Uruguay, using the recommended amount with incomplete Freund's adjuvant. The immune response was checked based on the number of antibodies produced by ELISA. In this part, the antibody titer is also important to determine the expected size of the nanobody library. After the clones were generated, an affinity enrichment process called panning would be necessary. In this case, phage display phagemid system 3+3 was used.

Selection of G9a-specific nanobodies was achieved in the same way as described above, where once the libraries were generated, phage display rounds were carried out. The library was first generated as stated before, by performing an amplification of 10 µL of M13 helper phage (New England Biolabs, USA, E8100S) in 1L tetracycline resistant ER2738 bacteria. The helper phage was incubated at 37ºC for 4h, with kanamycin (x1.4). Once the library generated, a plate was coated with antigen solution (5 µg per well of G9a) overnight in humid conditions and 4ºC. The next day, the antigen solution was removed, and the plate was blocked with 1% BSA at RT for 1h. Later, incubation with the nanobody-presenting phage library was carried out (1.74×10^{10} phages). The unbound phages were later removed by washing with PBS+0.1% Tween 20 and

the ones that remained bound were eluted with 10 µg/mL Trypsin for 30 minutes at 37ºC. Finally, the phage output was tittered and amplified after every round; the amplification was carried out by infecting ER2738 bacteria in SB + 100 mg/mL ampicillin medium with the phage output at 37ºC until OD_{600} 0.6 was achieved. Later, the output was amplified by M13 helper phage + ampicillin for 2h at 37ºC, and finally overnight in SB + kanamycin. The amplified phages were subsequently precipitated with 20% PEG and tittered in kanamycin Petri dishes. Four consecutive panning rounds were performed in the case of the nanobody library, and the output/input ratio was used as an enrichment indicator.

Once the minimum panning rounds were reached and the desired enrichment was observed, screening assays were performed by growing cultures of isolated clones (monoclonality) and evaluating nanobody binding to their antigen in an ELISA assay. In this assay the recognition capacity of different VHHs towards the target protein was evaluated through the expression of recombinant VHHs clones isolated from viral particles. 26 colonies were selected at random from the unamplified titer plates of the fourth panning round and grown in LB + ampicillin medium at 37ºC.

Cultures were then induced with IPTG (2 mM) and maintained in the induction state for 16 hours to maximize VHH production in the periplasm and to reach the steady state of culture growth. The bacteria were later centrifuged and the supernatant containing enough VHHs for screening was collected. An indirect ELISA assay was performed to analyze the VHHs-rich supernatant, and the ELISA plates were sensitized with HBsAg or HBcAg. The supernatant of each VHH clone was loaded into the wells and incubated for 1h. Then, the supernatant was removed and the anti-HA-peroxidase antibody was added (Sigma-Aldrich®). After plate reveal, the VHHs that were specific for the antigen of interest were considered ‘positive’, while non-specific VHHs were considered ‘negative’. This classification was made according to the reveal color they showed (positive clones) or did not show (negative clones), and to their absorbance value at 450 nm.

3.7 BioPROTAC design and evaluation

After evaluating the peptides from Nanotemper, the next step was the generation and design of the BioPROTAC construction. Subsequently, the BioPROTAC activity was meant to be evaluated in different cell lines to observe the degradation of G9a by Western Blot, as well as its internalization in the cell through immunocytochemistry (ICQ) at different dilutions. ICQ could be performed in this research, while Western Blot remains as a future perspective for the project.

The BioPROTAC construct (**Figure 6**) was designed with one of the selected peptides (7 amino acids), a glycine and serine linker, a VHL ligand, and an arginine-rich peptide. The selected peptide acts as POI binding domain, and the VHL ligand as an E3 ligase binding domain. On the other hand, the arginine-rich peptide was used as a strategy for cell-penetration (37) and the whole construct was labeled with FITC for ICQ visualization, as recommended in bibliographical research.

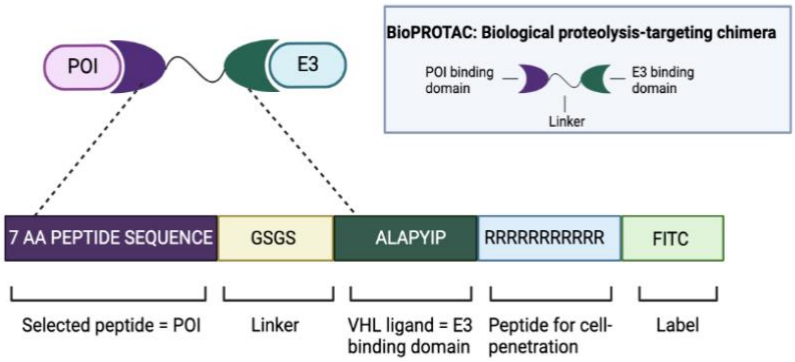

Figure 6. BioPROTAC designed construct*. It is composed of a POI binding domain which is the selected 7 aa peptide, and an E3 binding domain which is the VHL ligand, followed by a peptide penetration peptide; the sequence was labeled with FITC.*

3.8 Immunofluorescence microscopy

To investigate the distribution of peptides and their interactions with targeted POIs, we utilized FITC-labeled peptides to locate the targeted proteins. All experimental procedures were conducted under dark conditions. Four chambers were prepared with HeLa cells at a density of 120,000 cells/well. Cells were fixed on coverslips in 4% paraformaldehyde at room temperature for 20 minutes and permeabilized for 15 minutes using 0.3% Triton-X100. Following multiple

rinses with PBS, cells were incubated with the synthesized BioPROTACs for 20 minutes, followed by DAPI (Biolegend®) for 1 h to observe the nuclei, at a final concentration of 25 µM each. After washing with PBS the cells were visualized and imaged using a Nikon Eclipse Ni-U microscope (Nikon, Japan) equipped with a high-definition camera, ProgRes MFcool (Jenoptik AG, Germany).

4. RESULTS AND DISCUSSION

4.1 G9a production in bacteria

4.1.1 Competent bacteria cultures

Competent bacteria were first produced as indicated in the Materials and Methods section, for the purpose of efficiently introducing the G9a plasmid DNA into them. After that, transformation of competent cells with the plasmid was carried out by heat shock and electroporation (**Figure 7**).

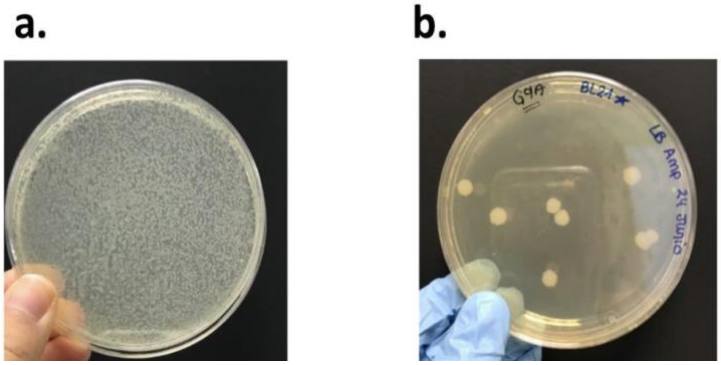

Figure 7. Bacterial transformation*. a: LB and ampicillin plate of bacteria transformed by electroporation. b: LB and ampicillin plate of bacteria transformed by heat shock.*

In order to standardize the bacteria transformation process, the calculation of Transformation Efficiency (TE) of both processes was necessary. TE is described as the number of colony forming units (CFU) seen per 1 µg of plasmid DNA used, as illustrated in the equation of **Figure 8**:

$$\boldsymbol{TE\ (cfu/\mu g) = (Number\ of\ colonies)\ /\ plasmid\ DNA\ (\mu g)}$$

Figure 8. *Mathematical equation used for transformation efficiency calculation (Figure adapted from* (38)*).*

Heat shock TE

Four different conditions were tested for TE calculation, to verify whether the number of colonies was proportional to the amount of plasmid used (**Figure 9**).

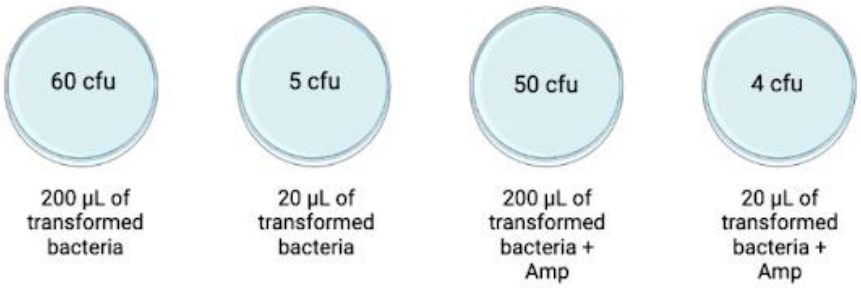

Figure 9. Different conditions tested for TE calculation. *2 of the plates were set up with 200 µL of transformed bacteria, and a 1:10 dilution of those bacteria was added onto the other 2 plates to prove proportionality of CFU.*

In 2 of the plates, ampicillin was added due to the pET-15b resistance to it. At the same time, 2 plates were set up with a 1:10 dilution of the mixture used in the other 2. Proportionality was observed in the results, leading to the conclusion of a successful transformation with 20-25% efficiency (**Table 2**).

	CFU	**µg of plasmid, [10 ng/µL]**	**TE (CFU/µg)**
No antibiotic added	60	2	30
No antibiotic added	5	0.2	25
Antibiotic added	50	2	25
Antibiotic added	4	0.2	20

Table 2. Necessary data for TE calculation. *The formula in* ***Figure 8*** *was used for TE calculation, taking into account the CFU number and the µg of plasmid used, which was at a final concentration of 10 ng/µL.*

4.1.2 Protein production in bacteria

Transformed bacteria were put onto a Petri dish of LB with 100 µg/mL ampicillin. Subsequently, a large-scale bacterial culture was made in LB + ampicillin medium (100 µg/mL), and later different conditions for protein expression induction with IPTG were tried (**Table 3**).

Time (h)	Temperature (ºC)	IPTG concentration (mM)	OD_{600}	Volume needed (µL), V_f = 1 mL
4	37	0 (negative control)	0.60	590
Overnight	18	0.3	1.08	328
4	18	0,3	1.17	300
Overnight	18	0,5	1.20	290
4	18	0,5	1.06	328
Overnight	37	0,5	1.06	328
4	37	0,5	0.73	480
Overnight	18	0,8	1.03	340
4	18	0,8	1.03	340

Table 3. Protein expression induction optimization. *Different time, temperature and concentration conditions were tested. Overnight or 4h IPTG induction was tried, at 3 different temperatures and 3 different IPTG concentrations. The optic density (OD) of the cultures was also measured and adjusted with the corresponding dilutions shown in the last column of the table.*

A G9a expression comparison was desired, so the optic density (OD) of bacteria was measured to know how much volume was needed for a posterior acrylamide gel with equal bacteria quantities (**Table 3, Figure 10**).

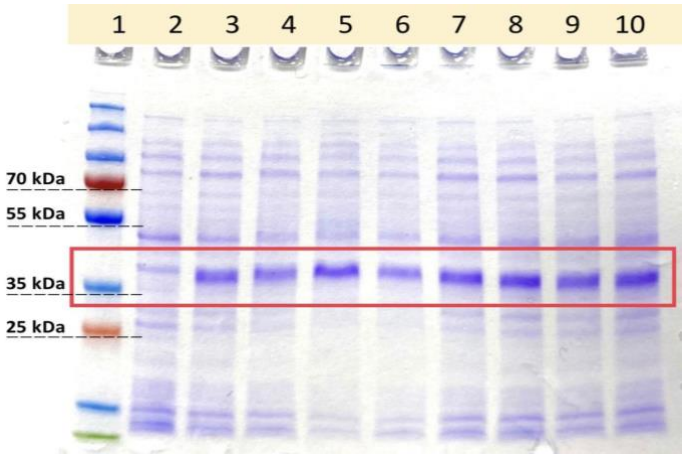

Figure 10. Comparison of different induction conditions. *1: MWM PageRuler #26619. 2: BL21 bacteria before IPTG induction. 3: IPTG 0.3 mM, overnight at 18ºC. 4: IPTG 0.3 mM, 4h at 18ºC. 5: IPTG 0.5 mM, overnight at 37ºC. 6: IPTG 0.5 mM, 4h at 37ºC. 7: IPTG 0.8 mM, overnight at 18ºC. 8: IPTG 0.8 mM, 4h at 18ºC. 9: IPTG 0.5 mM, overnight at 18ºC. 10: IPTG 0.5 mM, 4h at 18ºC.*

GenScript® construction is based on the catalytic domain of G9a, whose weight with the added tag is 35.02 kDa (306 aa). There was a clear overexpressed band visible at the expected weight of a 35 kDa protein without any degradation products for all different conditions, as well as no visible G9a in the negative control (BL21 bacteria before IPTG induction). The same overexpression in SDS-Page could be observed for all conditions, indicating that changes in culture size, media, or IPTG concentration have no impact on the expression result. When the temperature is reduced, cellular processes slow down, resulting in reduced rates of transcription and translation. The slowing down of cellular processes should result in fewer degradation products, correct protein folding, and increased solubility. Therefore, the chosen condition for further occasions was 18°C, overnight.

4.1.3 Corroboration of G9a presence before the purification process

Corroborating G9a presence after protein expression induction was an important checkpoint in the project. Before moving on to the purification of the protein, G9a expression had to be assured so as not to purify in vain. G9a expression of 6 batches was evaluated previous to their purification; all of them showed the desired expression (**Figure 11**) so a good protein production process was guaranteed and the subsequent purification was initiated. In **figure 11**, samples before and after IPTG induction are observed.

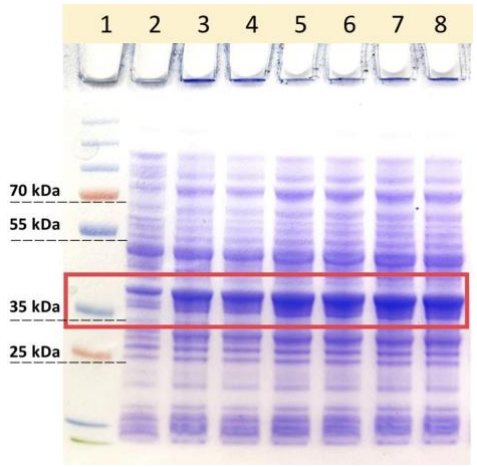

Figure 11. SDS-PAGE gel of G9a presence corroboration. *1: MWM PageRuler #26619. 2: BL21 bacteria before IPTG induction. 3 to 8: BL21 bacteria after IPTG induction. At the same time, in this gel different G9a production batches were present; 2 and 3: production batch 1 (1L). 4: production batch 2 (1L). 5: production batch 3 (1L). 6: production batch 4 (1L). 7: production batch 5 (1L). 8: production batch 6 (1L).*

Clearly, at the expected weight of 35 kDa, overexpression of G9a was observed in all the post-induction samples, (lanes 3 to 8 in the gel), compared to the pre-induction sample (lane 2 in the gel). This meant a successful protein expression induction, with the target protein ready to be purified.

4.2 Protein purification

4.2.1 Purification by Immobilized Metal Affinity Chromatography (IMAC)

In IMAC, protein purification is achieved by the affinity of metal ions (Ni^{2+}, in this case) to surface-accessible histidine residues. Purification of the recombinant G9a that had been produced was based on that affinity principle since it contained a polyhistidine tag.

For the elution of the protein, a linear gradient (0%-4%-20%-40%-100%) of a competitive inhibitor for histidine-tagged proteins was used: 750 mM imidazole. The resulting chromatogram (**Figure 12**) showed various separated peaks on each of the imidazole concentrations. Later on, an SDS-PAGE gel showed how G9a always elutes when the imidazole concentration in the elution buffer is 300 mM (40%).

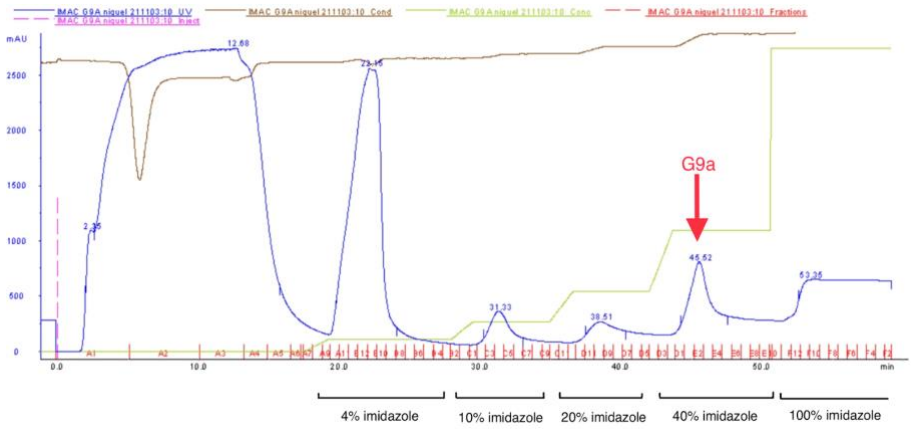

Figure 12. IMAC purification of G9a. *Chromatogram showing G9a eluted when the imidazole concentration is 300mM (40%).*

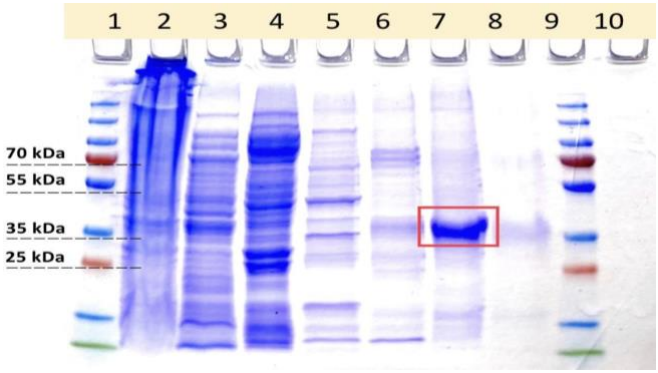

Figure 13. SDS-PAGE gel of IMAC chromatography result. *1: MWM PageRuler #26619. 2: BL21 bacteria after French Press lysis. 3: Column flowthrough 4: First elution peak of IMAC (4% imidazole) 5: Second elution peak of IMAC (10% imidazole). 6: Third elution peak of IMAC (20% imidazole). 7: Fourth elution peak of IMAC (40% imidazole). 8: Last elution fractions (100% imidazole). 9: MWM PageRuler #26619.*

The vast majority of the G9a protein appeared at a competitive inhibitor concentration of 300mM of imidazole, as seen in lane 7 of the gel (**Figure 13**) and as indicated in the chromatogram's fourth elution peak (**Figure 12**).

In addition, bacteria before IMAC purification were included in lane 3 (BL21 after lysis), to be able to compare how the column separates the different proteins of the sample. Apart from the expected G9a bands, other protein bands were visible too, indicating that after IMAC purification of the protein, there are still contaminants remaining. This is due to the fact that IMAC is not able to separate proteins based on size or shape. The fraction where G9a seemed to be present was collected for further purification by size-exclusion chromatography.

4.2.2 Purification by gel filtration (GF)

Gel filtration or size exclusion chromatography is often used as a subsequent step to IMAC, to further separate and purify the target protein. Overall, the gel in **Figure 15** shows that complementation of IMAC and gel filtration techniques was successful, obtaining a higher purity of the target protein without any visible bands other than the ones of G9a.

In a size exclusion chromatography, the first elution peaks correspond to the biggest proteins. In this case, G9a is observed in the second elution peak of GF, and additional elution peaks were observed. The latter peaks corresponded to smaller compounds, such as the imidazole and buffer salts that the equipment was also capable of separating.

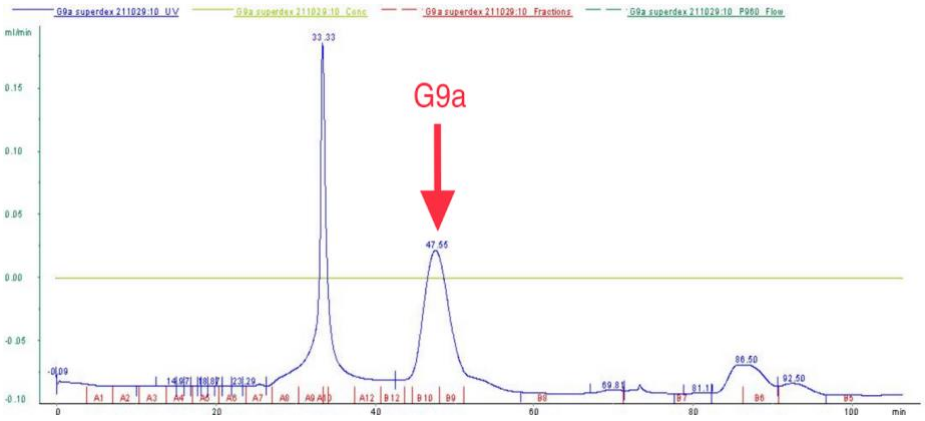

Figure 14. GF purification of G9a. *Size exclusion chromatogram showing G9a in the second elution peak.*

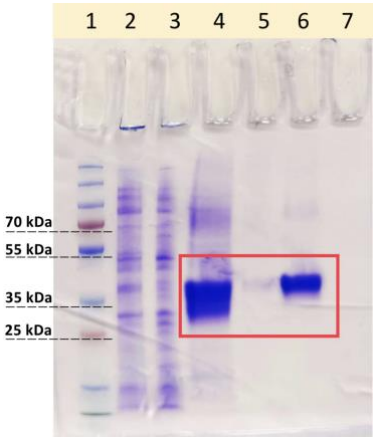

Figure 15. SDS-PAGE gel of GF chromatography result. *1: MWM PageRuler #26619. 2: BL21 bacteria before IPTG induction. 3: BL21 bacteria after IPTG induction, 18ºC overnight. 4: G9a after IMAC purification. 5: First elution peak of GF (A9, A10 fractions). 6: Second elution peak of GF, where G9a is observed (B9, B10 fractions). 7: Last elution peak of GF.*

4.2.3 Protein quantification by BCA assay

G9a was produced in four different batches, and the protein that had been produced and purified from each of the four batches was quantified using the BCA assay. A standard curve was obtained using serial dilutions of BCA and the slope of the curve was used to interpolate the protein quantity of the four batches (**Figure 16, Table 4**).

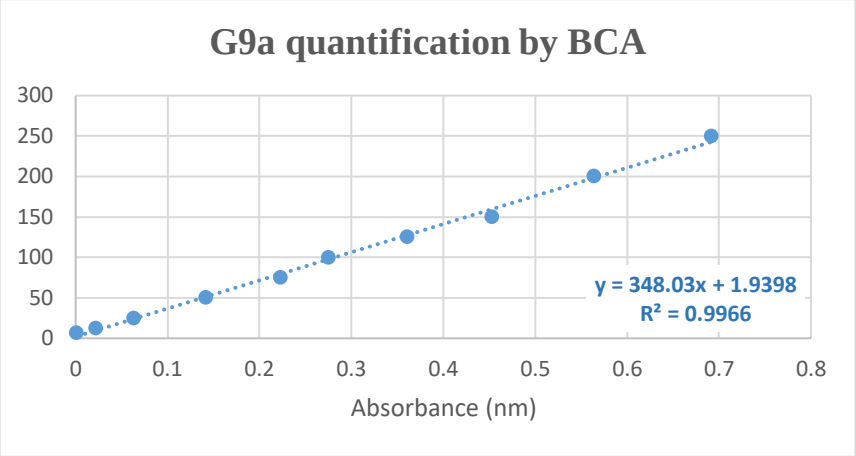

Figure 16. Standard curve obtained in the BCA assay*; absorbance (nm) vs. protein quantity (µg), with an R2 value of 0.9966.*

Results in **table 4** show how the first and fourth protein production batches were the ones that generated the most protein quantity. The first batch had been produced with heat shocked BL21 bacteria, while the fourth batch was with electroporated BL21 bacteria. This meant that no significant production differences could be observed between both transformation methods in terms of protein quantity, and none of them was selected as preferred for future experiments.

Protein concentration (µg/mL)	Batch 1	Batch 2	Batch 3	Batch 4
Without dilution	272.86	198.11	224.14	247.99
Dilution 1:2	147.46	94.86	122.44	149.00
Dilution 1:4	72.55	38.29	57.08	68.84

Table 4. Protein quantity obtained for each protein production batch. *Protein quantity was measured without dilution of the sample, dilution 1:2 and dilution 1:4. The protein concentrations in the table are expressed in µg/mL.*

4.3 Target protein activity assay

Afterward, an activity assay was carried out to prove whether the G9a produced in each of the four batches had enzymatic activity or not. In this assay, the fractions whose activity was measured (**Figure 17**) were the ones that had been purified by IMAC and GF in each of the production batches.

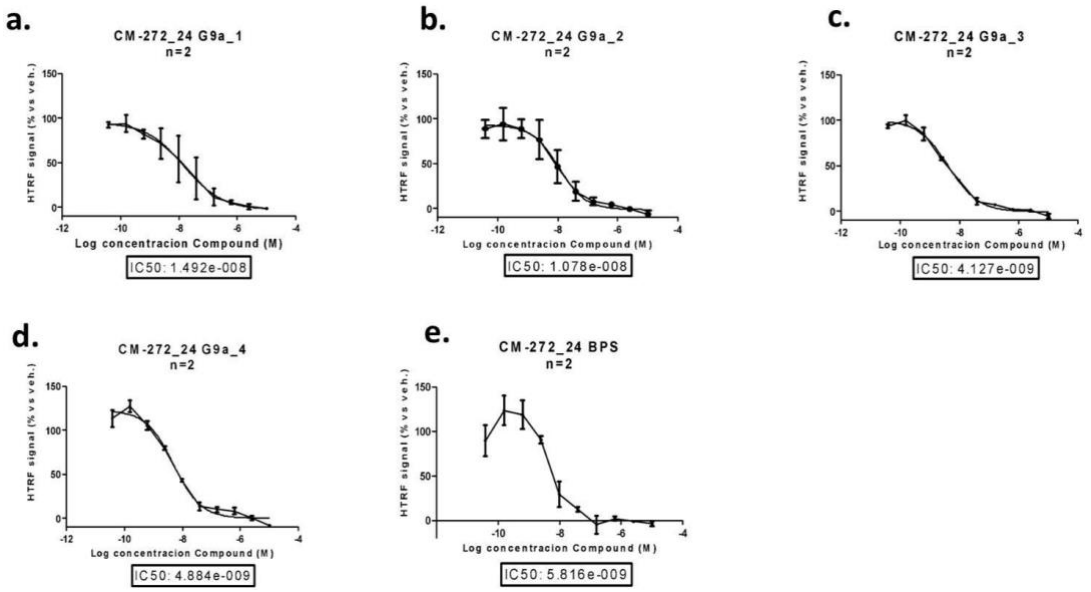

Figure 17. Graph results of G9a activity assay*. a: G9a purified derived for batch 1. b: G9a purified derived for batch 2. c: G9a purified derived for batch 3. d: G9a purified derived for batch 4. e: commercial G9a.*

The biochemical assay to measure G9a enzyme activity relies on time-resolved fluorescence energy transfer (TR-FRET). The activity assay was based on the use of a G9a-selective inhibitor compound: CM-272. Every well contained the same amount of enzyme G9a and decreasing concentrations of CM-272 were added in order to obtain an IC50 value.

This IC50 value was correlated with the activity of the enzyme. Usually, the lowest IC50 possible is desired, because a lower IC50 indicates a more potent compound. However, in the case of these activity assays, a higher half maximal inhibitory concentration is convenient since better G9a activity means that more inhibitor compound is needed to reach zero enzyme activity.

Results of the activity assay in **Figure 17, a-d** suggest that the recombinant G9a that had been produced and purified continued to have enzymatic activity. More specifically, batches 1 and 2

(**Figure 17, a and b**, respectively) had the highest activity (1.492e-008 M, and 1.078e-008 M, respectively). IC50 values of the four batches were additionally compared with the commercially available G9a (**Figure 17, e**), finding out that the activity of the protein produced in the laboratory was better than that of the commercial one. This allowed for high reliability in the production, purification, and subsequent selection processes of peptides and nanobodies.

4.4 Phage display

After each of the four panning rounds, a titration of the phage output was performed with serial dilutions. This step was crucial to later calculate an output/input ratio that was used as an enrichment indicator. This was important because enrichment in phage display means an increase in proportion of the phages that bind to the target, thereby obtaining more specificity of the output. The same procedure was followed for both peptides (NEB Ph.D-7 library) and nanobodies selected by phage display.

4.4.1 Panning rounds: titration results for NEB Ph.D-7 library

Serial dilutions (1:10) of the phage output obtained in panning round 2 of peptides were carried out in order to titer the number of phages for the consequent panning round (**Figure 18**). In the plates that correspond to dilutions -1, -2 and -4, the number of CFU was uncountable. On the other hand, in the plate with dilution -6 800 CFU were observed, and in the plate with dilution -7 138 CFU were counted. However, the acceptable range for CFU counting is 25-250, so dilution -7 was chosen for titer calculation.

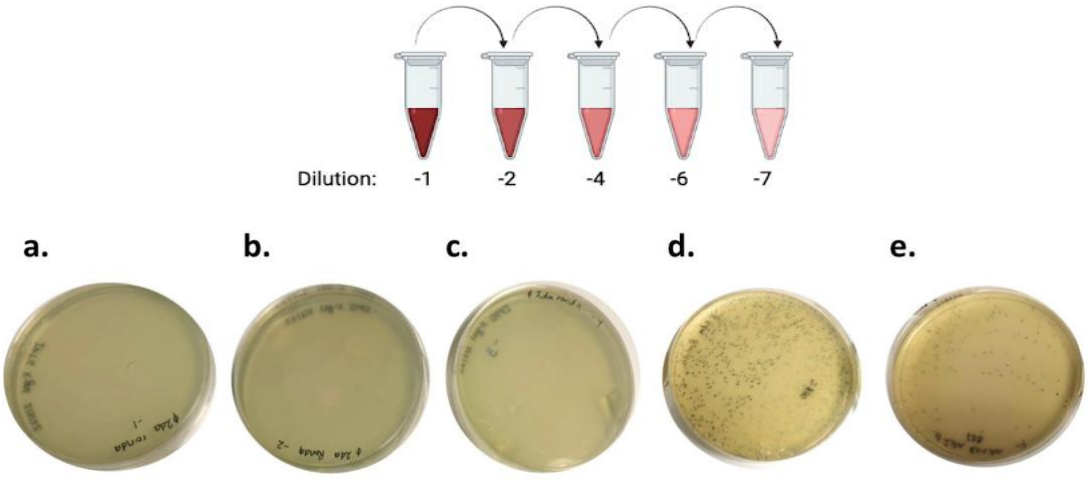

Figure 18. Titration example of the phage output obtained in panning round 2 of peptides. *Plates a to e correspond to dilutions -1, -2, -4, -6, and -7, respectively.*

Additionally, another three plates with serial dilutions (1:10) of the output were set up in order to obtain a more specific phage titer (**Table 5**). In this case, 10 µL of the output were put directly over the plate obtaining 146 CFU. Dilutions -1 and -2 of this same mixture resulted in 15 and 1 CFU, respectively. Proportionality in the dilutions was observed, making phage output titration reliable, and allowing to make the corresponding dilution for the input of the consequent panning round 3.

Output of the 2nd panning round	Amplified output of the 2nd panning round
10 µL: 146 CFU	-1 dilution: uncountable CFU
-1 dilution: 15 CFU	-2 dilution: uncountable CFU
-2 dilution: 1 CFU	-4 dilution: uncountable CFU
	-6 dilution: 800 CFU
	-7 dilution: 138 CFU

Table 5. Summary of the output dilutions of the second panning round. *Both the output and the amplified output of the second panning round were titrated, making serial dilutions of the eluted phages.*

4.4.2 Enrichment of NEB Ph.D-7 library

Firstly, the output of each panning round was calculated taking into account the number of colonies of each titration plate, which was multiplied by the dilution factor used in each case. As for the input, it was the same for every round as previously mentioned: 2×10^{11}. With these data, the output/input ratio was calculated to see whether enrichment of the peptide library had occurred among the panning rounds (**Table 6**). As seen in **Figure 19**, the proportion of the specific phages that bind to the target had increased. Therefore, the main objective of phage display was achieved; various clones with binding specificity for G9a had been obtained.

	Input	Output	Output/Input
Round 1	2×10^{11}	2.4×10^{5}	1.2×10^{-6}
Round 2	2×10^{11}	1.4×10^{5}	7×10^{-6}
Round 3	2×10^{11}	2.9×10^{6}	1.4×10^{-5}

Table 6. Enrichment of NEB Ph.D-7 library. *Data from the number of phages in the input and output of the 3 panning rounds from NEB Ph.D-7 library.*

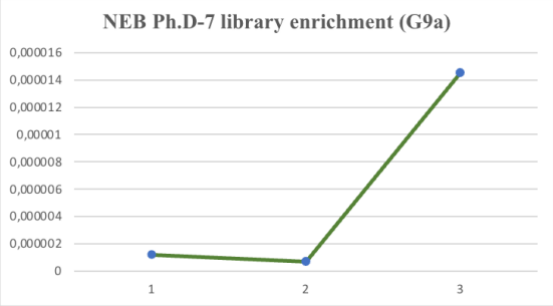

Figure 19. Graph showing enrichment of the G9a-specific clones from NEB Ph.D-7 library. *Results from the output/input ratio of the 3 panning rounds are shown. A great enrichment of specific clones was observed between rounds 2 and 3, concluding that in the latter round enough clone titer had been obtained.*

4.4.3 Screening of NEB Ph.D-7 library

Once enrichment of specific clones had been observed, each clone was evaluated individually in a screening assay or phage ELISA. The plate was coated with G9a, so the higher the absorbance result, the higher the binding of the peptide should be. In this case, for example, clones 5 and 24 show high binding results in the screening assay. This process was performed in order to select the best candidates for BioPROTAC construction synthesis. Specifically, 3 of the peptides were selected and later evaluated by Nanotemper.

In addition, another plate was coated with 1% BSA and the same peptide clones were evaluated individually on it to explore possible binding unspecificities against BSA. Absorbance results on the graph of **Figure 20** show that the binding for G9a of the peptides (columns in blue) is higher than the binding of BSA (columns in orange), concluding that good peptide candidates had been selected.

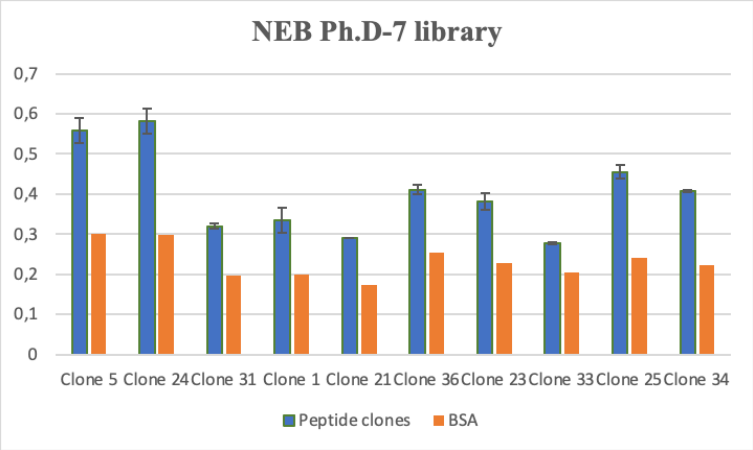

Figure 20. Peptide screening in search for G9a-binding peptides. *Results on the graph show side-by-side absorbance results for the peptide clones evaluated against G9a (blue), and for the peptide clones against BSA (orange).*

4.4.4 Panning rounds: titration results for nanobody library

The same procedure as with the peptide library was followed for the nanobody library generated by llamas immunization with G9a. In this case, titration of phages was carried out before panning round 1, and after each of the 4 panning rounds performed (**Figure 21**).

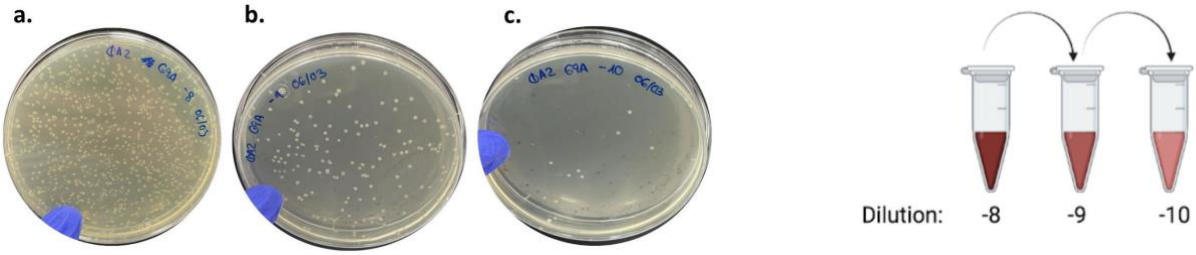

Figure 21. Titration example of the phage output obtained in panning round 2 of nanobodies. *Plates a to c correspond to dilutions -8, -9 and -10, respectively.*

4.4.5 Enrichment of nanobody library

Output calculation from nanobody panning rounds was done equally to the peptide library; the number of colonies of each titration plate was multiplied by the dilution factor used in each case. This time, the input from round 1 corresponded to the VHH antibody (nanobody) titer

generated by llamas immunization. In the following panning rounds, the input was standardized to 2×10^{11} to be able to establish an output/input ratio (**Table 7**).

After 4 panning rounds, the tendency observed was an increase in G9a-specific clones, meaning that clone-enrichment was also successful for the nanobody library (**Figure 22**).

	Input	Output	Input/Output
Round 1	1.74×10^{10}	7×10^{3}	4.02×10^{-7}
Round 2	2.23×10^{11}	6.4×10^{5}	2.86×10^{-6}
Round 3	2×10^{11}	7×10^{5}	3.5×10^{-6}
Round 4	2×10^{11}	1.9×10^{7}	9.5×10^{-5}

Table 7. Enrichment of nanobody library. *Data from the number of phages in the input and output of the 4 panning rounds from nanobody library.*

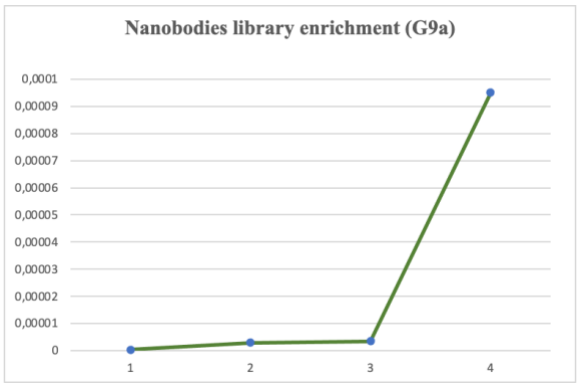

Figure 22. Graph showing enrichment of the G9a-specific clones from nanobody library. *Results from the output/input ratio of the 4 panning rounds are shown. A great enrichment of specific clones was observed between rounds 3 and 4, concluding that in the latter round enough clone titer had been obtained.*

4.4.6 Screening of nanobody library

Finally, nanobody clones were individually evaluated in a screening assay following the same procedure as with the peptide clones. The higher the absorbance result, the higher the binding of the nanobody to G9a should be. In this case, for example, clones 4 and 20 show high binding

results in the screening assay. The best candidates (16, specifically) were consequently selected for sequencing and BioPROTAC construct design.

Equally to the peptide library, an additional ELISA plate was set up with 1% BSA instead of G9a, in order to explore possible binding unspecificities against BSA. Absorbance results on the graph of **Figure 23** show that the binding for G9a of the nanobodies (columns in blue) is much higher than the binding of BSA (columns in orange), concluding that the nanobody specificity was against G9a and not BSA.

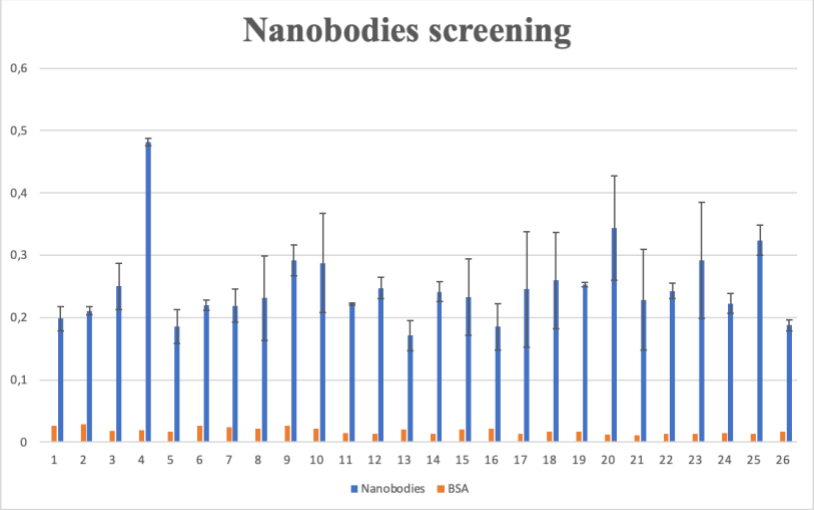

Figure 23. Nanobody screening in search for G9a-binding nanobodies. *Results on the graph show side-by-side absorbance results for the nanobody clones evaluated against G9a (blue), and for the nanobody clones against BSA (orange).*

4.5 Binding assay: Nanotemper

Ligand binding to the target protein causes changes in fluorescence intensity (**Figure 24**), which are measured by the MST equipment. At the same time, a brief laser-induced temperature change is applied. That variation in fluorescence is then plotted against the concentration of the target protein to obtain a dissociation constant (Kd) value, as well as the standard deviation of the duplicate indicated by error bars.

The lower the Kd value, the higher the affinity of the ligand for the target protein. Accordingly, Kd values obtained (**Table 8**) suggest that peptide 5 has a good affinity for G9a. Additionally,

the signal-to-noise ratio (SNR) was obtained for each peptide. The higher the SNR, the better the signal quality, since the desired signal is more distinguishable from the noise. This means that the most reliable measurement was the one from peptide 5, coinciding with the best Kd result (228.43uM). MST results led to think that a good candidate for G9a binding was peptide 5, despite the fact that all 3 peptides show binding. However, it is necessary to corroborate the results with other binding techniques such as SPR (Superficie Plasmon Resonance) or Octet technique.

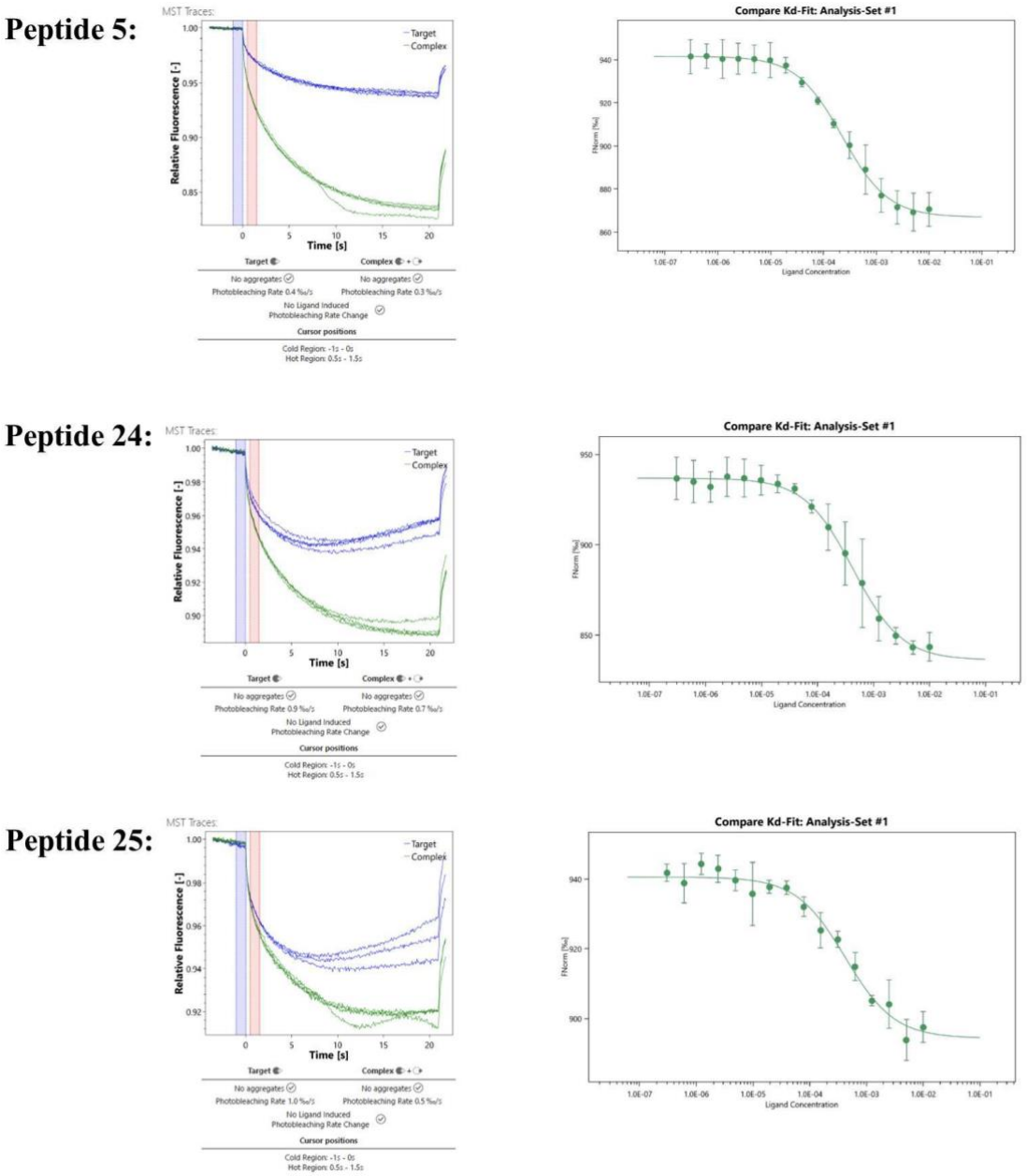

Figure 24. Nanotemper results for peptides 5, 24 and 25. *For each peptide, a graph showing changes in fluorescence intensity between target (G9a) and complex (G9a + peptide) is displayed. Additionally, a graph showing each peptide's dissociation curve is shown.*

	Kd (µM)	SNR (dB)
Peptide 5	228.43	54.33
Peptide 24	430.93	50.42
Peptide 25	423.93	19.20

Table 8. MTS results for the peptides. *In this table dissociation constant (Kd) and Signal-to-noise ratio values obtained for each of the peptides tested in Nanotemper are shown.*

4.6 Immunocytochemistry

As proof of concept, different BioPROTAC concentrations were used as treatment over the cells (**Figure 25**), to observe the interaction of the construct with an *in vitro* tumor environment. Taking into account that the targeted POI is located intracellularly (specifically near the nucleus for its binding to euchromatic regions), cell permeabilization was carried out as specified in the materials and methods section; an additional control was set up without cell permeabilization, but no significant differences were observed.

The permeabilization step had the purpose of slightly disrupting the cell membrane structure and therefore facilitating the internalization of the construct. The results obtained show that cell permeabilization worked efficiently, allowing the BioPROTAC to enter the cell via the arginine peptide for cell-penetration. All of the BioPROTAC concentrations exhibited some internalization of the construct into the cells; nuclei are shown in blue (stained with DAPI) and BioPROTACs are seen in green (labeled with FITC). However, the BioPROTAC concentration at which the best internalization results were observed was 2.5 µM. Additionally, direct proportionality between the concentration of the construct added and the number of green spots seen was reflected. This meant having overcome one of the biggest drawbacks of the BioPROTAC system: cell-internalization capability.

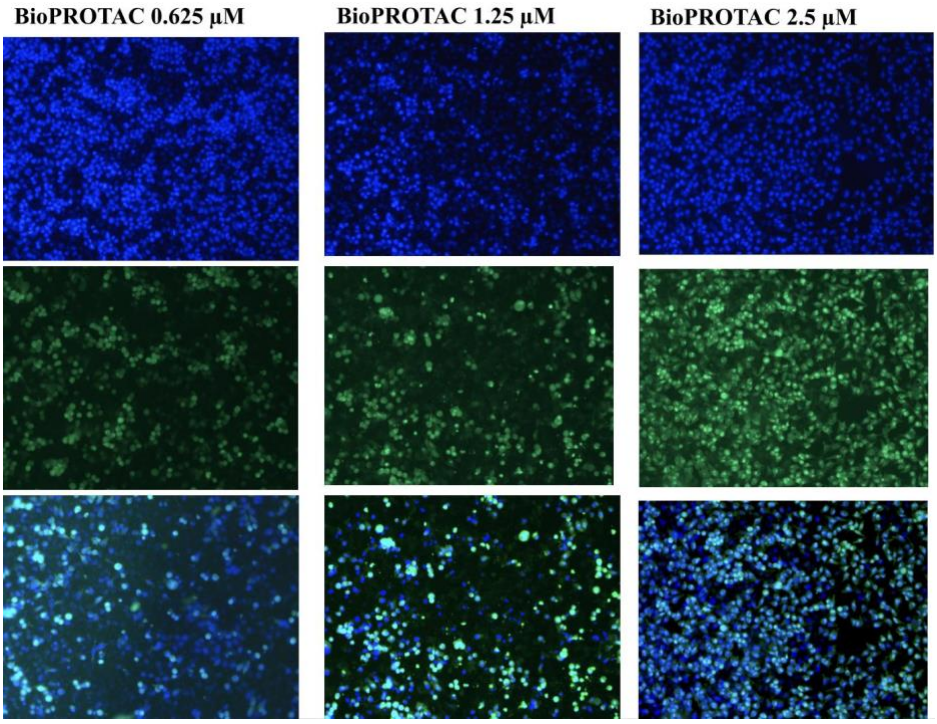

Figure 25. ICQ to study cell internalization. *HeLa cells were treated with three different BioPROTAC concentrations: 0.625, 1.25 and 2.5 µM. Cells are observed in blue and the construct in green; the third row in the figure shows how the construct was successfully internalized into HeLa cells.*

5. CONCLUSIONS

As a general conclusion, it could be said that the main objectives of the research project were carried out successfully. Firstly, the target protein (G9a) was produced into the pET-15b vector by a bacterial expression system. This protein was consequently purified by chromatographic techniques in four different batches, obtaining better results when G9a was purified by two subsequent IMAC and GF chromatographies. Four different batches of the protein were produced, purified and quantified; batches number 1 and 4 had the highest protein quantity (272.86 µg/mL and 247.99 µg/mL, respectively). The bacteria used in these two batches had been transformed by heat shock (batch 1) and by electroporation (batch 4), so protein quantification results demonstrated that one transformation method was not better than the other in terms of protein quantity. The produced G9a batches were later evaluated in an enzymatic activity assay, where batches 1 and 2 demonstrated to have the highest activity (IC50 1: 1.492e-008 M, IC50 2: 1.078e-008 M). Moreover, the catalytic activity of the produced protein (in all the batches) was even higher than that of the commercial G9a (IC50: 5.816e-009 M).

Once the first objectives of the project met, the produced target protein was used in phage display for G9a-specific peptide and nanobody selection. In fact, 10 peptide clones and 26 nanobody clones were firstly selected as candidates for G9a binding, from which 3 peptides and 16 nanobodies were finally selected by affinity assays (ELISA). To corroborate affinity of the peptides, these 3 final candidates were evaluated by Nanotemper. All of them showed binding to their target, but peptide 5 was the one that showed the best result in Nanotemper (Kd: 228.43 µM). Finally, this research project addressed one of the biggest challenges presented by BioPROTACs when used as therapeutic molecules: cell-permeability. Through immunocytochemistry, cell-internalization of the synthesized BioPROTAC was best demonstrated at a final construct concentration of 2.5 µM with permeabilized HeLa cells.

In summary, the main goal of the study was achieved: G9a-specific peptides and nanobodies identification for protein degradation complex (BioPROTAC) design. Secondary objectives were also accomplished, except for BioPROTAC effect evaluation in tumor cell lines to see whether G9a is degraded or not. This is seen as an opportunity to continue the research of this project and therefore develop a new potential therapeutic approach for cancer with numerous advantages over existing therapies.

The BioPROTAC consists of a circular ubiquitin-proteasome system (UPS) that is continuously recycled and can take part in several cycles of protein degradation. This means that treatment with PROTAC technology is capable of overcoming several aspects that are considered to be a limitation of traditional protein inhibitors. To start with, BioPROTAC recycling allows using low quantities of the construct (sub-stoichiometric concentrations), even if the POI is highly expressed. Therefore, it can be concluded that the constant availability of the construct implies that $DC_{50} > IC_{50}$, again meaning an advantage of BioPROTACs over protein inhibitors. In addition, this TPD system is able to solve another of the main concerns that inhibitor drugs involve: drug resistance. In case of mutations in the catalytic domain of the POI, an inhibitor would probably lose its function because they mostly act over the active site of the protein (27). This would result in the development of resistance to the drug, which can be overcome by BioPROTACs due to their capability to target different sites in the protein. In essence, this emerging TPD technology has bright perspectives toward achieving an alternative treatment in cancer.

6. LIMITATIONS AND FUTURE PERSPECTIVES

Limitations

It is worth noting that this project has some limitations, and that taking them into account is necessary to put in perspective the direction of the research. BioPROTACs have already shown great potential in preclinical and early clinical trials (**Table 1**). However, some limitations of this technology should be mentioned to fully consider their therapeutic scope.

In the first place, selectivity for the target protein is one of the biggest challenges with PROTACs. Although a search for high selectivity is done through successive panning rounds, lack of specificity of the small peptides and nanobodies is still plausible leading to off-target effects.

On the other hand, the reliability of Nanotemper results is not very high. It is true that binding is observed, but a slight change of the conditions proved a highly different Kd in every case. Therefore, other techniques with which robust binding values and affinity can be demonstrated are necessary. Examples of these techniques are the SPR (Surface Plasmon Resonance) and the Octet technique.

Future perspectives

As stated before, the very next step to be accomplished in this project would be G9a degradation verification. For this, treatment of tumor cell lines should be done at different BioPROTAC concentrations and time, as well as subsequent protein extraction to perform a Western Blot (WB). Successful results would show a G9a quantity decrease over time.

On the other hand, all the possible G9a analog molecules should be analyzed to see if the selected peptides and nanobodies have similar properties toward them. This would enable refinement of the selection in order to avoid binding of the PROTAC to molecules with high homology to G9a such as GLP (euchromatic histone-lysine N-methyltransferase 1, EHMT1) (39).

In line with refinement of the peptide and nanobody selection, another of the future perspectives of the project is to develop sub-libraries of the final phage display output obtained for both peptides and nanobodies. Generation of sublibraries consists in introducing random point mutations into the sequence of the selected clones that are already known to have selectivity for the target. This could result in finding selective candidates with the possibility to have increased affinity for the POI. In short, refinement of phage selection would be to perform a secondary screening over the clones selected in the first place.

Looking ahead, if G9a degradation WB hypothetically demonstrated promising results, clinical translation of BioPROTACs should be the main concern. Firstly, different BioPROTAC doses should be evaluated in order to study possible differences in POI degradation. This study would allow further tests of the Targeted Protein Degradation system *in vivo*; safety and toxicity concerns should be taken into account, as well as pharmacokinetics of the construct (solubility, stability and half-life of the PROTAC in the organism), and delivery into the tumor microenvironment. In short, there is no doubt that there is still a long way to go to achieve a functional G9a degradation system, as well as an improvement of current cancer prospects toward a more personalized and effective medicine.

7. APPENDIX: ABBREVIATIONS

TPD: Targeted protein degradation

H3K4: Lysine 4 of histone 3

H3K9: Lysine 9 of histone 3

EHMT2: Euchromatic histone-lysine N-methyltransferase 2

PROTAC: Proteolysis-targeting chimera

POI: Protein of interest

E3: E3 ubiquitin ligase

VHL: Von Hippel-Lindau tumor suppressor

CRBN: Cereblon

DC_{50}: degradation concentration 50

IC_{50}: inhibitory concentration 50

LYTACs: Lysosome-targeting chimeras

AbTACs: Antibody-targeting chimeras

O'PROTACs: Oligonucleotide-based PROTACs

BioPROTAC: Biological Proteolysis Targeting Chimera

OD: Optic density

TE: Transformation efficiency

CFU: Colony forming unit

IPTG: Isopropyl ß-D-1-thiogalactopyranoside

TMB: Tetramethylbenzidine

TR-FRET: Time-resolved fluorescence energy transfer

RT: room temperature

SNR: signal-to-noise ratio

ICQ: Immunocytochemistry

HBsAg: Hepatitis B surface antigen

HBcAg: Hepatitis B core antigen

WB: Western Blot

MWM: Molecular weight marker

8. BIBLIOGRAPHY

1. Bray F, Laversanne M, Weiderpass E, Soerjomataram I. The ever-increasing importance of cancer as a leading cause of premature death worldwide. Cancer. 2021 Aug 15;127(16):3029–30.
2. Torre LA, Siegel RL, Ward EM, Jemal A. Global cancer incidence and mortality rates and trends - An update. Vol. 25, Cancer Epidemiology Biomarkers and Prevention. American Association for Cancer Research Inc.; 2016. p. 16–27.
3. Abudu R, Bourougaa K, Bouche Gauthier. Trends in International Cancer Research Investment 2006-2018. American Society of Clinical Oncology. 2021.
4. Sadikovic B, Al-Romaih K, Squire JA, Zielenska M. Cause and Consequences of Genetic and Epigenetic Alterations in Human Cancer. Vol. 9, Current Genomics. 2008.
5. Hayashi-Takanaka Y, Yamagata K, Wakayama T, Stasevich TJ, Kainuma T, Tsurimoto T, et al. Tracking epigenetic histone modifications in single cells using Fab-based live endogenous modification labeling. Nucleic Acids Res. 2011 Aug;39(15):6475–88.
6. Dawson MA, Kouzarides T. Cancer epigenetics: From mechanism to therapy. Vol. 150, Cell. Elsevier B.V.; 2012. p. 12–27.
7. Cedar H, Bergman Y. Linking DNA methylation and histone modification: Patterns and paradigms. Vol. 10, Nature Reviews Genetics. 2009. p. 295–304.
8. A M De Marzo, V L Marchi, E S Yang, R Veeraswamy, X Lin, W G Nelson. Abnormal regulation of DNA methyltransferase expression during colorectal carcinogenesis - PubMed. 1999 Aug.
9. Robertson KD, Uzvolgyi E, Liang G, Talmadge C, Sumegi J, Gonzales FA, et al. The human DNA methyltransferases (DNMTs) 1, 3a and 3b: coordinate mRNA expression in normal tissues and overexpression in tumors. Vol. 27, Nucleic Acids Research. 1999.
10. Caldas C, Venkitaraman A. Tumor Suppressor Gene Related terms: Approaches to Identification. 2001.
11. Esteller M. Cancer epigenomics: DNA methylomes and histone-modification maps. Vol. 8, Nature Reviews Genetics. 2007. p. 286–98.
12. Roth SY, Denu JM, David Allis C. HISTONE ACETYLTRANSFERASES [Internet]. 2001. Available from: www.annualreviews.org
13. Greer EL, Shi Y. Histone methylation: A dynamic mark in health, disease and inheritance. Vol. 13, Nature Reviews Genetics. 2012. p. 343–57.
14. Souza BK, Freire NH, Jaeger M, de Farias CB, Brunetto AL, Brunetto AT, et al. EHMT2/G9a as an epigenetic target in pediatric and adult brain tumors. Int J Mol Sci. 2021 Oct 1;22(20).
15. Chen MW, Hua KT, Kao HJ, Chi CC, Wei LH, Johansson G, et al. H3K9 histone methyltransferase G9a promotes lung cancer invasion and metastasis by silencing the cell adhesion molecule Ep-CAM. Cancer Res. 2010 Oct 15;70(20):7830–40.
16. Zhang C, Wei S, Hu J, Xiong Z, Lee JH. Upregulated expression of G9a is correlated with poor prognosis of gastric cancer patients. Medicine (United States). 2019 Nov 1;98(48).

17. Egger G, Liang G, Aparicio A, Jones PA. Epigenetics in human disease and prospects for epigenetic therapy [Internet]. Los Angeles; 2004. Available from: www.nature.com/nature

18. Barski A, Cuddapah S, Cui K, Roh TY, Schones DE, Wang Z, et al. High-Resolution Profiling of Histone Methylations in the Human Genome. Cell. 2007 May 18;129(4):823–37.

19. Meng CF, Zhu XJ, Peng G, Dai DQ. Re-expression of methylation-induced tumor suppressor gene silencing is associated with the state of histone modification in gastric cancer cell lines. World J Gastroenterol. 2007;

20. Wozniak RJ, Klimecki WT, Lau SS, Feinstein Y, Futscher BW. 5-Aza-2′-deoxycytidine-mediated reductions in G9A histone methyltransferase and histone H3 K9 di-methylation levels are linked to tumor suppressor gene reactivation. Oncogene. 2007 Jan 4;26(1):77–90.

21. Zhang J, He P, Xi Y, Geng M, Chen Y, Ding J. Down-regulation of G9a triggers DNA damage response and inhibits colorectal cancer cells proliferation [Internet]. Vol. 6, Oncotarget. 2020. Available from: www.impactjournals.com/oncotarget/

22. Hua KT, Wang MY, Chen MW, Wei LH, Chen CK, Ko CH, et al. The H3K9 methyltransferase G9a is a marker of aggressive ovarian cancer that promotes peritoneal metastasis. Mol Cancer. 2014 Aug 9;13(1).

23. Tai KY, Shiah SG, Shieh YS, Kao YR, Chi CY, Huang E, et al. DNA methylation and histone modification regulate silencing of epithelial cell adhesion molecule for tumor invasion and progression. Oncogene. 2007 Jun 7;26(27):3989–97.

24. Liu XR, Zhou LH, Hu JX, Liu LM, Wan HP, Zhang XQ. UNC0638, a G9a inhibitor, suppresses epithelial-mesenchymal transition-mediated cellular migration and invasion in triple negative breast cancer. Mol Med Rep. 2018 Feb 1;17(2):2239–44.

25. Li Q, Wang L, Ji D, Bao X, Tan G, Liang X, et al. BIX-01294, a G9a inhibitor, suppresses cell proliferation by inhibiting autophagic flux in nasopharyngeal carcinoma cells. 2021; Available from: www.graphpad.com

26. Rahman Z, Rabi Bazaz Mohd, Devabattula G. Targeting H3K9 methyltransferase G9a and its related molecule GLP as a potential therapeutic strateg. J Biochem Mol Toxicol. 2020;

27. Moreira-Silva F, Outeiro-Pinho G, Lobo J, Guimarães R, Gaspar VM, Mano JF, et al. G9a inhibition by CM-272: Developing a novel anti-tumoral strategy for castration-resistant prostate cancer using 2D and 3D in vitro models. Biomedicine and Pharmacotherapy. 2022 Jun 1;150.

28. Poso A. The Future of Medicinal Chemistry, PROTAC, and Undruggable Drug Targets. Vol. 64, Journal of Medicinal Chemistry. American Chemical Society; 2021. p. 10680–1.

29. Li X, Song Y. Proteolysis-targeting chimera (PROTAC) for targeted protein degradation and cancer therapy. Vol. 13, Journal of Hematology and Oncology. BioMed Central Ltd.; 2020.

30. Qi SM, Dong J, Xu ZY, Cheng XD, Zhang WD, Qin JJ. PROTAC: An Effective Targeted Protein Degradation Strategy for Cancer Therapy. Vol. 12, Frontiers in Pharmacology. Frontiers Media S.A.; 2021.

31. Békés M, Langley DR, Crews CM. PROTAC targeted protein degraders: the past is prologue. Vol. 21, Nature Reviews Drug Discovery. Nature Research; 2022. p. 181–200.

32. Buhimschi AD, Armstrong HA, Toure M, Jaime-Figueroa S, Chen TL, Lehman AM, et al. Targeting the C481S Ibrutinib-Resistance Mutation in Bruton's Tyrosine Kinase Using PROTAC-Mediated Degradation. Biochemistry. 2018 Jul 3;57(26):3564–75.

33. Banik SM, Pedram K, Wisnovsky S, Ahn G, Riley NM, Bertozzi CR. Lysosome-targeting chimaeras for degradation of extracellular proteins. Nature. 2020 Aug 13;584(7820):291–7.

34. Cotton AD, Nguyen DP, Gramespacher JA, Seiple IB, Wells JA. Development of Antibody-Based PROTACs for the Degradation of the Cell-Surface Immune Checkpoint Protein PD-L1. J Am Chem Soc. 2021 Jan 20;143(2):593–8.

35. Shao J, Yan Y, Ding D, Wang D, He Y, Pan Y, et al. Destruction of DNA-binding proteins by programmable O'PROTAC: Oligonucleotide-based PROTAC. 2021; Available from: https://doi.org/10.1101/2021.03.08.434493

36. Mooney JT, Fredericks DP, Zhang C, Christensen T, Jespergaard C, Schiødt CB, et al. Purification of a recombinant human growth hormone by an integrated IMAC procedure. Protein Expr Purif. 2014;94:85–94.

37. Dai MY, Shi YY, Wang AJ, Liu XL, Liu M, Cai HB. High-potency PD-1/PD-L1 degradation induced by Peptide-PROTAC in human cancer cells. Vol. 13, Cell Death and Disease. Springer Nature; 2022.

38. Liu J, Chang W, Pan L, Liu X, Su L, Zhang W, et al. An Improved Method of Preparing High Efficiency Transformation Escherichia coli with Both Plasmids and Larger DNA Fragments. Indian J Microbiol. 2018 Dec 1;58(4):448–56.

39. Kubicek S, O'Sullivan RJ, August EM, Hickey ER, Zhang Q, Teodoro MLL, et al. Reversal of H3K9me2 by a Small-Molecule Inhibitor for the G9a Histone Methyltransferase. Mol Cell. 2007 Feb 9;25(3):473–81.